ACS NANO

www.acsnano.org

ARTICLE

Positive-Type Reversibly Photoswitching Red Fluorescent Protein for Dual-Color Superresolution Imaging with Single Light Exposure for Off-Switching

Ryohei Ozaki-Noma, Tetsuichi Wazawa, Taishi Kakizuka, Hisashi Shidara, Kiwamu Takemoto, and Takeharu Nagai*

Cite This: *ACS Nano* 2025, 19, 7188–7201

Read Online

ACCESS | Metrics & More | Article Recommendations | Supporting Information

ABSTRACT: **Positive-type reversibly photoswitching fluorescent proteins (p-rsFPs) transition to a bright on-state upon light exposure for fluorescence excitation and to a dark off-state under a different wavelength. p-rsFPs are widely used in superresolution (SR) imaging techniques, offering simplified observation procedure and enhanced biocompatibility. Although some green p-rsFPs possess adequate photoproperties for SR imaging, all red p-rsFPs (p-rsRFPs) to date exhibit suboptimal properties, limiting the color palette for multiplexed SR imaging. Here, we present a p-rsRFP, rsZACRO, with 3.0-fold brighter fluorescence, 5.3-fold faster off-switching, and 1.5-fold higher on/off contrast than rsCherry, a conventional representative p-rsRFP. Using rsZACRO with superresolution polarization demodulation/on-state polarization angle narrowing (SPoD-OnSPAN), we successfully demonstrated SR imaging in the red spectrum and dual-color SR imaging with a single light for off-switching, visualizing vimentin intermediate filaments and actin filaments at higher spatial resolution than the diffraction limit of light in a living mammalian cell.**

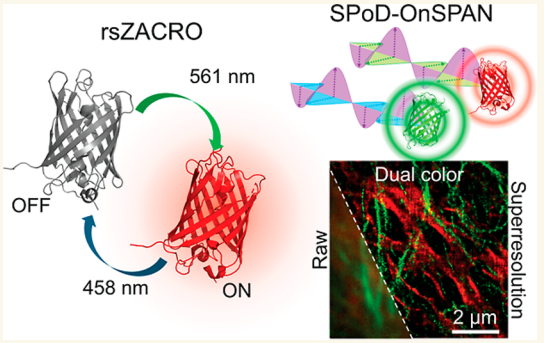

KEYWORDS: *fluorescence, positive-type reversibly photoswitching fluorescent protein, red fluorescent protein, chromophore phenolate, multiple equilibria, superresolution imaging, nanoscopy*

INTRODUCTION

Reversibly photoswitching fluorescent proteins (rsFPs) are a class of genetically encodable fluorescent proteins that can reversibly switch between a fluorescently bright state (on-state) and a fluorescently dark state (off-state) upon light irradiation.[1] rsFPs are categorized into negative- and positive-types. Negative-type rsFPs (n-rsFPs) transition from the on to the off-state upon irradiation with light for fluorescence excitation (off-switching) and from the off to the on-state with light at another wavelength (on-switching). In contrast, positive-type rsFPs (p-rsFPs) undergo on-switching with light for fluorescence excitation and off-switching with light at another wavelength. The photoswitching of both n-rsFPs and p-rsFPs is believed to involve the cis−trans isomerization of the chromophore, along with the protonation and deprotonation of its phenol group in the β-barrel.[2−4] rsFPs have been applied to various techniques, including molecular tracking,[5] optomanipulation,[6] optical lock-in detection,[7,8] detection of multiple fluorescence signals in single channel,[9−13] measurement of cellular activities,[14−17] extension of fluorescence anisotropy measurement to large molecular complexes,[18] and particularly, superresolution (SR) imaging.[19]

SR imaging allows for the visualization of minute intracellular structures at a spatial resolution beyond the diffraction limit of light.[19] Specifically, SR imaging techniques employing rsFPs include reversible saturable optical linear transitions (RESOLFT),[20,21] nonlinear structured illumination microscopy (NL-SIM),[22] and photochromic stochastic optical fluctuation imaging (pcSOFI).[23] In addition, superresolution

Received: November 23, 2024
Revised: January 29, 2025
Accepted: January 30, 2025
Published: February 12, 2025

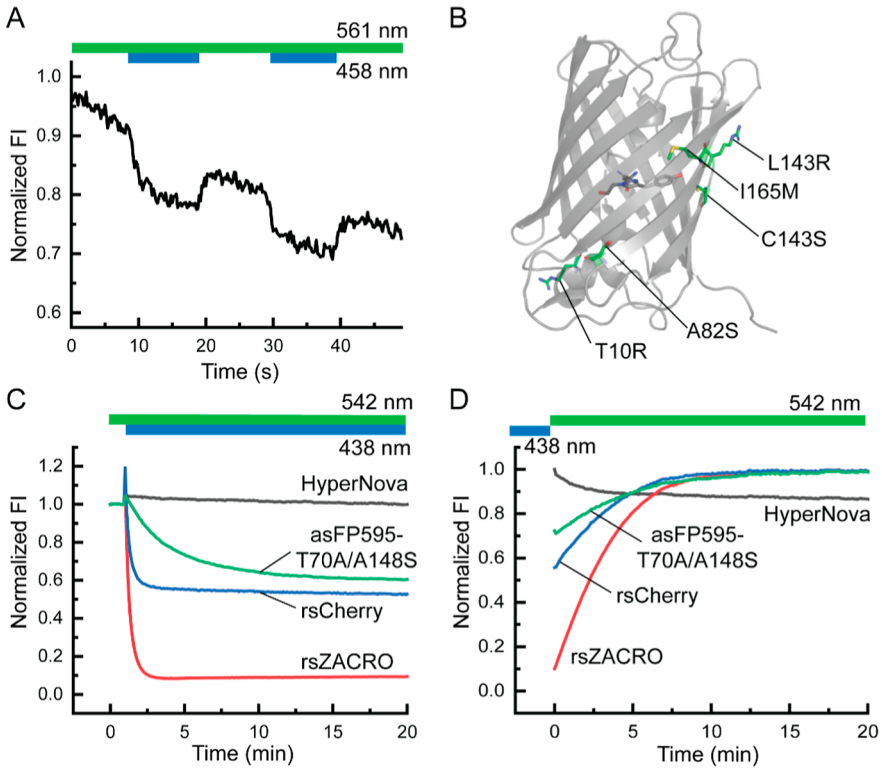

Figure 1. Development of rsZACRO. (A) Time trajectory of normalized fluorescence intensity for vimentin-HyperNova in HeLa cells, subjected to continuous illumination at 561 nm and intermittent irradiation at 458 nm. Irradiation power densities were 1.0 W/cm^2 at 561 nm and 10 mW/cm^2 at 458 nm. (B) Locations of mutations introduced into HyperNova to derive rsZACRO, shown on the structure of its precursor, SuperNova, (PDB ID, 3WCK).[41] (C) Fluorescence response to a 438 nm light in the presence of a 542 nm light for HyperNova (black), rsCherry (blue), asFP595-T70A/A148S (green), and rsZACRO (red) expressed in *E. coli* cells. Cells were initially exposed to 542 nm, followed by simultaneous irradiation with 542 and 438 nm. (D) Fluorescence response to stopping 438 nm light exposure while continuing 542 nm light for these FPs. The initial exposure was to 438 nm, followed by 542 nm. The 542 nm light served for fluorescence excitation and on-switching, and the 438 nm light for off-switching. Power densities were 2.6 mW/cm^2 at 542 nm and 1.7 mW/cm^2 at 438 nm. FI denotes fluorescence intensity.

polarization demodulation/excitation polarization angle narrowing (SPoD-ExPAN) is an SR imaging technique that resolves oriented fluorophores using linearly polarized lights for excitation and stimulated emission depletion (STED).[24] However, the required power density of STED light exceeds 10^6 W/cm^2, leading to significant phototoxicity in living cells. We thereupon devised a technique to circumvent these issues by exploiting the nonlinear fluorescence response of Kohinoor and Kohinoor2.0 p-rsFPs, avoiding the use of STED light.[25−27] Consequently, we developed a highly biocompatible SR imaging technique known as SR polarization demodulation/on-state polarization angle narrowing (SPoD-OnSPAN). In fact, we successfully performed SR imaging using SPoD-OnSPAN with illumination at a significantly reduced power density of approximately 1 W/cm^2.[25−27] p-rsFPs are also used in RESOLFT and NL-SIM techniques, characterized by significantly low power densities of irradiation light and simplified irradiation sequences.[28−30] However, the currently available p-rsFPs with adequate photoproperties for live cell SR imaging are limited to green-fluorescence variants, specifically Kohinoor2.0 and Padron2.[27,29]

Positive-type reversibly photoswitching red fluorescent proteins (p-rsRFPs) are anticipated to enable multicolor SR imaging and live cell imaging with reduced phototoxicity and enhanced observation depth.[31−34] To date, the developed p-rsRFPs include asFP595[35] and rsCherry.[32] Although asFP595 was initially used for the proof-of-concept of RESOLFT imaging *in vitro*,[20] proteins tagged with asFP595 have frequently been reported to mislocalize in cells due to oligomerization.[36] Although rsCherry is monomeric, its photoproperties are suboptimal for SR imaging with a fluorescence quantum yield (QY) of approximately 0.02 in the on-state and a photoswitching contrast of only 6.7 between the on- and the off-states.[32] Due to the suboptimal performance of existing p-rsRFPs as fluorescence tags, the color palette for SR observation remains limited, and achieving dual-color SR imaging remains challenging; therefore, there is a need to develop a p-rsRFP with brighter fluorescence and higher on/off contrast for SR imaging.

In this study, we developed a p-rsRFP, rsZACRO, suitable as a fluorescent tag for SR imaging. rsZACRO exhibits higher fluorescence intensity, faster off-switching speeds, and greater on/off contrast in mammalian cells compared to the conventional p-rsRFP, rsCherry. To develop rsZACRO, we conducted directed evolution using HyperNova[37] as the starting material and screened the variants by monitoring their fluorescence intensity and on/off contrast. We demonstrated dual-color SPoD-OnSPAN imaging in live mammalian cells using rsZACRO and Kohinoor2.0,[27] employing single light irradiation for off-switching. This approach enabled us to visualize the fine structures of vimentin intermediate filaments and actin filament networks within the same field of view.

https://doi.org/10.1021/acsnano.4c16847
ACS Nano 2025, 19, 7188−7201

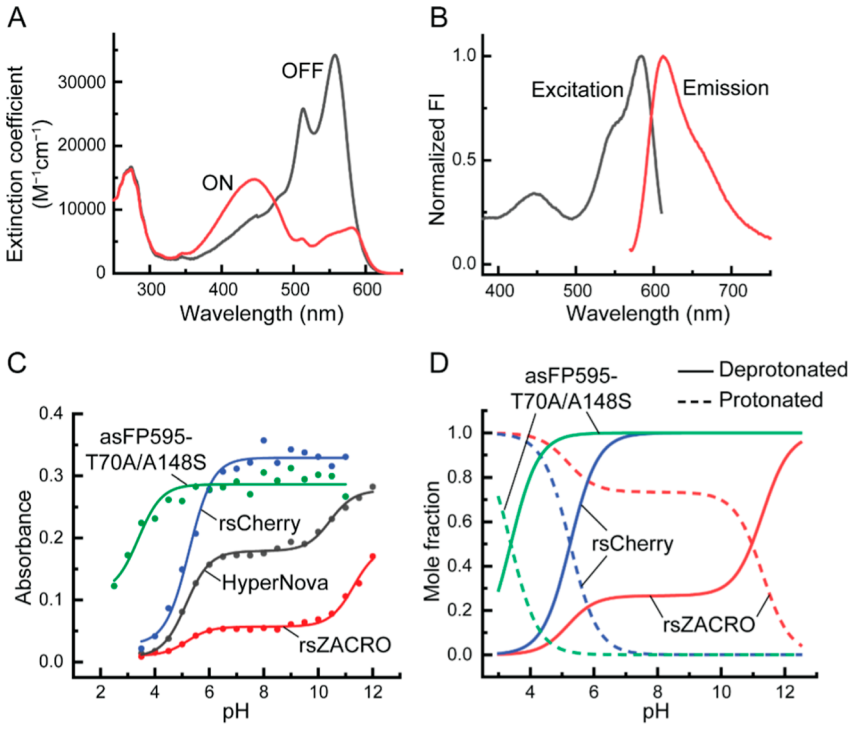

Figure 2. Photophysical properties of rsZACRO *in vitro*. (A) Spectral extinction coefficients for rsZACRO in the on-state (red) and the off-state (black). (B) Fluorescence emission and excitation spectra of rsZACRO in the on-state, with the excitation wavelength for the emission spectrum set at 560 nm, and the emission wavelength for the excitation spectrum set at 630 nm. (C) pH-dependent absorption profiles for HyperNova, rsCherry, asFP595-T70A/A148S and rsZACRO, with respective absorbance wavelengths at 565, 570, 570, and 573 nm. rsCherry, asFP595-T70A/A148S, and rsZACRO were measured in the on-state. Solid lines for HyperNova and rsZACRO were model-derived (Supporting Information Figure S4B), while those for rsCherry and asFP595-T70A/A148S were based on a single protonation equilibrium model (n = 3). (D) pH-dependent mole fractions of protonated (dotted lines) and deprotonated (solid line) chromophore states for rsCherry, asFP595-T70A/A148S, and rsZACRO. FI denotes fluorescence intensity.

RESULTS AND DISCUSSION

Development of a Positive-Type Reversibly Photoswitching Red Fluorescent Protein, rsZACRO. We noticed that HyperNova, a red fluorescent photosensitizing protein,[37] exhibited a glimpse of positive-type reversible photoswitching in HeLa cells (Figure 1A). For SPoD-OnSPAN imaging with higher spatial and temporal resolution and greater biocompatibility, larger on/off contrast, higher fluorescence brightness, and faster on- and off-switching speed are critical requirements for p-rsFP. Considering these requirements, the low on/off contrast of HyperNova makes it unlikely to be suitable for SPoD-OnSPAN imaging (Figure 1A). Therefore, we decided to enhance the on/off contrast of HyperNova through directed evolution. HyperNova, derived from SuperNova,[38] which itself was developed from KillerRed,[39] incorporates A44-KR variant known to undergo light-induced cis−trans isomerization of the chromophore.[40−42] Consequently, we hypothesized that HyperNova's photoswitching mechanism similarly involves cis−trans isomerization of the chromophore, and conducted site-saturation mutagenesis on amino acids surrounding Tyr-66, a component of the chromophore, guided by the crystal structure of SuperNova (PDB ID, 3WCK).[38] Additionally, we introduced the T10R mutation, known to enhance chromophore maturation efficiency in SuperNova and KillerRed.[43] Subsequently, we cultured *Escherichia coli* (*E. coli*) cells transformed with the mutant cDNA library on LB agarose gel plates and monitored the fluorescence intensity and photoswitching contrast of each colony. These were measured as the ratio of fluorescence intensity under excitation at 542 nm to that under off-switching at 438 nm followed by additional excitation at 542 nm using an in-house-built illumination system (Supporting Information Figure S1A). Ultimately, we isolated a mutant (HyperNova-T10R/A82S/I143R/S145C/I163M) (Figure 1B) that exhibited a significantly higher photoswitching contrast than rsCherry, a representative conventional p-rsRFP,[32] and asFP595-T70A/A148S[35] in *E. coli* colonies (Figure 1C,D and Supporting Information Figure S1B). We denote the HyperNova variant as rsZACRO (for the primary sequence, see Supporting Information Figure S2).

Photophysical Properties of rsZACRO *In Vitro*. We analyzed the photoproperties of purified rsZACRO. At room temperature equilibrium, rsZACRO's absorption spectrum featured bands at 450 and 580 nm (peak wavelengths of 446 and 581 nm, respectively) (Figure 2A), which are attributed to the protonated and deprotonated states of the phenolic group in the chromophore, respectively.[2,4] In addition, we identified a minor nonfluorescent absorption band at 512 nm (Figure 2A,B), potentially due to anionic p-hydroxybenzylidene imidazolinone (a green chromophore), similar to DsRed.[44] Both the 580 and 450 nm bands were fluorescent, as confirmed by the excitation spectrum (Figure 2B); the fluorescence emission from the 450 nm band likely occurs through excited-state proton transfer (ESPT).[42,45] The quantum yield (QY) of rsZACRO when excited at 550−570 nm was measured to be 0.19, and its fluorescence brightness—calculated as the product of fluorescence quantum yield and molar extinction coefficient—was 3.5 times higher than that of rsCherry (Table

https://doi.org/10.1021/acsnano.4c16847
ACS Nano 2025, 19, 7188−7201

Table 1. Photophysical Properties of rsZACRO and Other FPs

protein	rsZACRO	rsCherry	HyperNova	asFP595-T70A/A148S
excitation/emission wavelength (nm)	584/612	591/614	576/607	578/603
extinction coefficient[a] (M^{-1} cm^{-1})	7200 (on, 581 nm) 34,200 (off, 558 nm)	40,200 (on, 572 nm)	30,500 (577 nm)	33,700 (on, 571 nm)
fluorescence quantum yield	0.19	0.01	0.32	0.04
brightness[b]	1400	400	9800	1300
maturation speed ($t_{1/2}$, min)	29.9	14.9	18.6	16.2
pK_a (pK_1/pK_2)	11.2/5.75	5.26	10.0/5.35	3.39
pL_H	10.7	N/A	10.2	N/A
k_{on} (s^{-1}, 561 nm/1 W/cm^2)	0.066	0.29	ND	ND
k_{off} (s^{-1}, 458 nm/10 mW/cm^2)	0.40	0.076	ND	ND
F_{on}/F_{off}[c]	10.1	6.85	ND	ND
photobleaching ($t_{1/2}$, s)	5.12	33.1	3.91	ND
photobleaching with periodic 458 nm light ($t_{1/2}$, s)	94.3	184.1	ND	ND

[a]The molar extinction coefficient for each protein was determined by measuring absorbance at the peak wavelength. Protein concentration was quantified using the BCA assay. [b]QY multiplied by the molar extinction coefficient. [c]F_{on} and F_{off} were determined based on fluorescence intensities after on-switching and off-switching, respectively, as shown in Supporting Information Figure S5. ND and NA stand for "not determined" and "not applicable," respectively.

1). Upon irradiation with 438 nm light, rsZACRO transitioned to the off-state, subsequently displaying two absorption bands at 558 and 512 nm (Figure 2A), corresponding to the chromophore phenolate and green chromophore, respectively. The half-time for oxygen-dependent maturation of rsZACRO was 29.9 min (Table 1 and Supporting Information Figure S3), indicating that rsZACRO is unsuitable for studies such as SR imaging of proteins with short half-lives. However, rsZACRO fluorescence can be observed if the target is not a short-lived protein, provided that sufficient time has elapsed after gene transfection.

We analyzed the pH-dependent absorption spectrum of rsZACRO and compared it with those of HyperNova, rsCherry, and asFP595-T70A/A148S to gain insight into the photoswitching mechanism of rsZACRO. We observed that the absorbance of the 580 nm band for these proteins increased with rising pH, whereas that of the 450 nm band decreased correspondingly (Supporting Information Figure S4A). These spectral changes likely reflect the pH-dependent equilibrium between the deprotonated (phenolate) and protonated (phenol) form of the chromophore.[4] Specifically, rsZACRO and HyperNova exhibited distinct pH-dependent behaviors compared to rsCherry and asFP595-T70A/A148S: the absorbance at 580 nm for rsZACRO increased with rising pH below pH 6 and above 9, but remained stable between pH 6 and 9 (Figure 2C). Additionally, as the pH increased from 9.5 to 12, the peak wavelength of the 580 nm band for rsZACRO shifted from 582 to 573 nm (Supporting Information Figure S4A). Analyzing the pH-dependent absorption alongside the protonation/deprotonation equilibrium of the chromophore's phenolic group,[27,46] we discovered that rsZACRO's chromophore phenolate protonation likely involves two pK_a values, pH-dependent, in contrast to the single pK_a value observed for the chromophore protonation in rsCherry and asFP595-T70A/A148S (Supporting Information Figure S4B, Table 1). The multiple pK_a values involved in the protonation of rsZACRO's chromophore phenolate at different pH levels facilitates an equilibrium between its phenol and phenolate forms (phenolate: phenol = 1:2.9−2.6) near neutral pH (pH 6.5−9) (Figure 2D), suggesting the protonated and deprotonated states of the rsZACRO chromophore in the on-state maintain a dynamic equilibrium with comparable mole fractions of them in the pH range between pK_1 (11.2) and pK_2 (5.75). The protonated state of chromophore, responsible for the 450 nm absorption band, allows rsZACRO to transition to the off-state (CH−X^- → OFF and CH−XH → OFF in Supporting Information Figure S4B) when excited. Furthermore, the deprotonated state of the chromophore spontaneously transitions to the protonated state (C^-−X^- → CH−X^- and C^-−XH → CH−X in Supporting Information Figure S4B), which, upon excitation at ∼450 nm, can also transition to the off-state. For reference, the mole fractions of protonated phenol at pH 7 were determined to be 1.8% and 0.024% for rsCherry and asFP595-T70A/A148S, respectively (Figure 2D). Therefore, we propose that the multiple protonation equilibrium of the rsZACRO chromophore plays a crucial role in its off-switching mechanism, contributing to a faster off-switching speed and higher on/off contrast compared to rsCherry. Similar pH-dependent multiple equilibrium behaviors of chromophore have also been observed in green p-rsFPs such as Kohinoor,[28] Kohinoor2.0[27] and Padron2,[29] where it was suggested that these equilibria involve a hydrogen bonding network including His-193, Glu-144, and Glu-211.[27] While the specific amino acids involved in the multiple protonation equilibrium of rsZACRO remain unidentified, further research into the amino acids surrounding the chromophore that participate in this pH-dependent equilibrium could yield invaluable insights for the rational design of high-performance p-rsFPs. Additionally, HyperNova, a photosensitizing fluorescence protein, also exhibits a multiple protonation equilibrium with a phenolate mole fraction of 0.63 at pH 7.0 (Supporting Information Figure S4C). It is important to note that the extinction coefficient of HyperNova at ∼580 nm, which significantly impacts the reactive oxygen species (ROS) production efficiency, depends on the mole fraction of the chromophore phenolate. Therefore, potential exists for further enhancing the ROS production efficiency of HyperNova by increasing the mole fraction of chromophore phenolate through mutagenesis, akin to the development of Kohinoor2.0.[27]

Properties of rsZACRO in Live Mammalian Cells. We investigated the photoswitching, photobleaching, fluorescence intensity, and phototoxicity of rsZACRO in live HeLa cells, aiming to apply it in cellular fluorescence imaging. To estimate

https://doi.org/10.1021/acsnano.4c16847
ACS Nano 2025, 19, 7188−7201

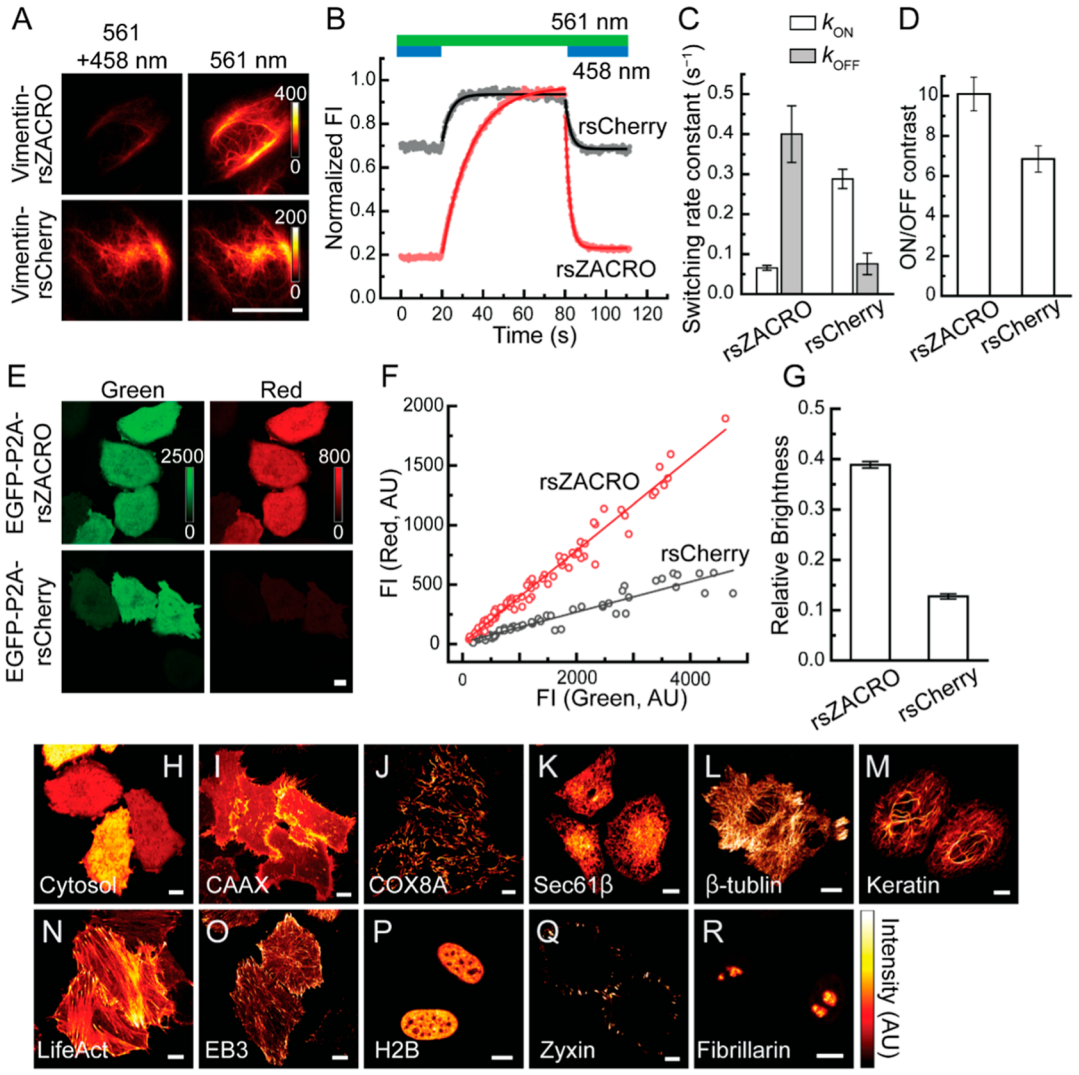

Figure 3. Properties of rsZACRO in live mammalian cells. (A) Fluorescence images of HeLa cells expressing vimentin-rsZACRO (upper panels) and vimentin-rsCherry (lower panels). Left panels: post off-switching with 458 and 561 nm irradiation; right panels: post on-switching with 561 nm irradiation. Images post off-switching and post on-switching are displayed at identical brightness and contrast setting for comparison. (B) Time trajectories of normalized fluorescence intensities for rsZACRO and rsCherry in HeLa cells under continuous irradiation at 561 nm and intermittent irradiation at 458 nm. Irradiation power densities were 1.0 W/cm^2 at 561 nm and 10 mW/cm^2 458 nm. (C) On- and off-switching rate constants for rsZACRO and rsCherry derived from (B) with respective power densities of 1.0 W/cm^2 and 10 mW/cm^2. Data are mean ± standard deviation (SD) (n = 5). (D) On/off contrasts for rsZACRO and rsCherry, as determined from Supporting Information Figure S5. Data are mean ± SD (n = 10). (E) Fluorescence images of ubiquitously expressed EGFP-P2A-rsZACRO (upper panels) and EGFP-P2A-rsCherry (lower panels) in HeLa cells, 44 h posttransfection. Left panels show EGFP fluorescence; upper right and lower right panels show rsZACRO and rsCherry fluorescence, respectively. Images in green and red channels are displayed at identical brightness and contrast setting for comparison. (F) Plots of red fluorescence intensity of rsZACRO and rsCherry against EGFP fluorescence. Sample sizes were 62 and 88 cells, respectively. Solid lines represent linear regressions used to calculate relative fluorescence intensities of rsZACRO and rsCherry to EGFP. (G) Fluorescence brightness of rsZACRO and rsCherry relative to EGFP derived from (F). Data are mean ± standard error. (H−R) Confocal fluorescence images showing unfused rsZACRO and rsZACRO fused with various localization tags and proteins in HeLa cells: (H) unfused rsZACRO (the intensity range; 0−1200 AU); (I) fusion with the *C*-terminal amino acids of K-Ras (CAAX) (the intensity range; 0−1500 AU); (J) fusion with targeting signal of cytochrome *c* oxidase subunit 8A (Cox8A) (the intensity range; 0−400 AU); (K) fusion with a subunit of the Sec61 translocon complex Sec61β (the intensity range; 0−800 AU); (L) rsZACRO fused with β-tubulin (the intensity range; 0−50 AU); (M) fusion with intermittent filament Keratin (the intensity range; 0−500 AU); (N) fusion with actin-binding peptide LifeAct (the intensity range; 0−2000 AU); (O) fusion with microtubule-associated protein of EB3 (the intensity range; 0−100 AU); (P) fusion with histone 2B (H2B); (the intensity range; 0−1000 AU) (Q) fusion with zinc-binding phosphoprotein Zyxin (the intensity range; 0−100 AU); (R) fusion with nucleolar protein Fibrillarin (the intensity range; 0−1000 AU). FI and AU stand for fluorescence intensity and arbitrary unit, respectively. Scale bars: 10 μm. The color scale bars are linear and normalized to the maximum intensity value (AU) of each 16 bit image.

photoswitching rates, we observed rsZACRO-labeled vimentin intermediate filaments (vimentin-rsZACRO) expressed in HeLa cells using a fluorescence microscope and measured the subsequent changes in fluorescence upon photoswitching (Figure 3A). During simultaneous irradiation at 561 nm for fluorescence excitation and on-switching, and 458 nm for off-switching, the fluorescence intensity of rsZACRO was initially low (0−20 s in Figure 3B). The fluorescence intensity of

https://doi.org/10.1021/acsnano.4c16847
ACS Nano 2025, 19, 7188−7201

rsZACRO increased over time once the off-switching light at 458 nm was turned off (20−80 s in Figure 3B), indicating the on-switching process of rsZACRO. Subsequently, the fluorescence intensity decreased when we resumed the irradiation with the off-switching light at 458 nm (80−110 s in Figure 3B), indicative of the relaxation to an equilibrium between the on- and off-states. Thereupon, we conducted least-squares fitting analysis on the fluorescence intensity time trajectory using single exponential functions to determine the rate constants for on- and off-switching (k_{on} and k_{off}, respectively), as we previously reported.[25] In addition, we measured the photoswitching of rsCherry in the same manner for comparison and found that rsZACRO's k_{on} and k_{off} were 4.4 times lower and 5.3 times higher, respectively, than those of rsCherry (Figure 3C and Table 1). Considering that the k_{off}/k_{on} ratio is critical for spatial resolution in SPoD-OnSPAN imaging,[25,26] rsZACRO appears more suitable for achieving high spatial resolution. However, the slower k_{on} could be a disadvantage for temporal resolution in SPoD-OnSPAN imaging, as this technique relies on the cycles of on- and off-switching of p-rsFPs. The on/off contrast ratios for rsZACRO and rsCherry, determined by comparing fluorescence intensities after off-switching and on-switching, were 10.1 and 6.85, respectively. The on/off contrast value for rsCherry was consistent with a previous report.[32] This indicates that rsZACRO's on/off contrast was 1.5 times higher than that of rsCherry (Figure 3D, Supporting Information Figure S5 and Table 1).

To examine photobleaching, we recorded changes in fluorescence intensity over time for vimentin-tagged rsZACRO, HyperNova, and rsCherry in HeLa cells under continuous light at 561 nm (Supporting Information Figure S6A). Fluorescence decay for rsCherry was modeled using a single exponential function, while decay for HyperNova and rsZACRO utilized a double exponential model, resulting in half-lives of 5.12 s for rsZACRO, 33.1 s for rsCherry, and 3.94 s for HyperNova, all measured at a power density of 10 W/cm^2. To investigate photoswitching fatigue, we monitored vimentin-rsZACRO expressed in HeLa cells under continuous 561 nm illumination and periodic intermittent light at 458 nm (Supporting Information Figure S6B). The data showed that rsZACRO photobleached faster than rsCherry during the photoswitching fatigue tests, yet rsZACRO's fluorescence responded more distinctly to intermittent 458 nm illumination than rsCherry's, even after significant photobleaching (inset in Supporting Information Figure S6B). This suggests a potential advantage of rsZACRO over rsCherry in SR imaging. Additionally, photobleaching under intermittent 458 nm light (Supporting Information Figure S6B) occurred significantly slower (half-life of 94.3 s for rsZACRO) compared to continuous light (half-life of 5.12 s for rsZACRO), even at the same 561 nm power density of 10 W/cm^2 (Supporting Information Figure S6A and Table 1). This result indicates that the off-state chromophore would be more resistant to photobleaching than the on-state chromophore. Considering that ROS generation upon chromophore excitation is responsible for photobleaching[47] and assuming that the on and off-states correspond to the cis and trans states of the rsZACRO's chromophore, respectively, the resistance of rsZACRO in the off-state to photobleaching aligns with findings from a previous study on amn2CP, an ancestor of KillerRed, and rsZACRO.[41] This previous study demonstrated that the amn2CP chromophore produced ROS with significantly lower efficiency than KillerRed, where the amn2CP and KillerRed chromophores predominantly exists in the trans and cis forms, respectively.[41]

To compare the fluorescence intensities of rsZACRO and rsCherry in mammalian cells, we transfected HeLa cells with a plasmid containing a fusion gene series comprising EGFP,[48] a self-cleaving P2A polypeptide,[49] and either rsZACRO or rsCherry p-rsRFP (EGFP-P2A-rsZACRO or EGFP-P2A-rsCherry). We expected that EGFP and p-rsRFP would be expressed in approximately equimolar ratios, remaining separate within the cells and thereby preventing FRET between EGFP and p-rsRFP. We confirmed the ubiquitous expression of rsZACRO and EGFP in HeLa cells (upper panels in Figure 3E), measured the fluorescence intensity of EGFP as a reference alongside that of rsZACRO in each cell, and plotted the fluorescence intensities of rsZACRO against EGFP for each cell (Figure 3F). Similarly, we measured the fluorescence intensity of rsCherry relative to EGFP using the same method (lower panels in Figure 3E,F). Figure 3F shows that the fluorescence intensities of rsZACRO and rsCherry are proportional to EGFP's; hence, we used EGFP fluorescence as an indicator of rsZACRO or rsCherry expression level in each cell. To quantitatively compare the fluorescence intensities of rsZACRO and rsCherry, we conducted a linear regression analysis on the data from Figure 3F to calculate the ratios of fluorescence intensity for rsZACRO and rsCherry relative to EGFP. Consequently, we found that the fluorescence intensity of rsZACRO in HeLa cells was 3.0-times higher than that of rsCherry (Figure 3G), closely aligning with the result of *in vitro* characterization (Table 1). Additionally, in our attempts to study asFP595-T70A/A148S, we were unable to confirm the presence of fluorescently labeled vimentin intermediate filaments; instead, we observed significant aggregates in HeLa cells transfected with the vimentin-asFP595-T70A/A148S gene (Supporting Information Figure S7A). Furthermore, the ubiquitous distribution observed with EGFP was absent in asFP595-T70A/A148S in HeLa cells transfected with the EGFP-P2A-asFP595-T70A/A148S gene (Supporting Information Figure S7B). These results suggest that oligomer formation by asFP595-T70A/A148S may have interfered with the proper localization of the tagged protein.[36] As a result, we decided not to continue further experiments with asFP595-T70A/A148S. Conversely, no such aggregates were observed in HeLa cells expressing either vimentin-rsZACRO or vimentin-rsCherry (Figure 3A and Supporting Information Figure S7A). Moreover, we confirmed the proper localization of rsZACRO fusion proteins and rsZACRO tagged with localization signals in HeLa cells (Figure 3H−R), demonstrating rsZACRO's compatibility with localization tags.

Phototoxicity of rsZACRO could be a concern in fluorescence live-cell imaging applications. Therefore, we assessed the phototoxicity of rsZACRO alongside HyperNova, mCherry, and EGFP in *E. coli* cells by measuring the rate of light-induced cell death in cells expressing these proteins.[39] The survival rate of cells expressing rsZACRO (53%) was comparable to that of cells expressing mCherry (59%), a commonly used red fluorescent protein in fluorescence imaging,[50] and was significantly higher than that of cells expressing HyperNova (13%) (Supporting Information Figure S8A). Additionally, we evaluated phototoxicity in HeLa cells by monitoring the localization of the Plekstrin homology (PH) domain, which detaches from the cell membrane upon inactivation by ROS.[39,51] We prepared HeLa cells transfected

https://doi.org/10.1021/acsnano.4c16847
ACS Nano 2025, 19, 7188−7201

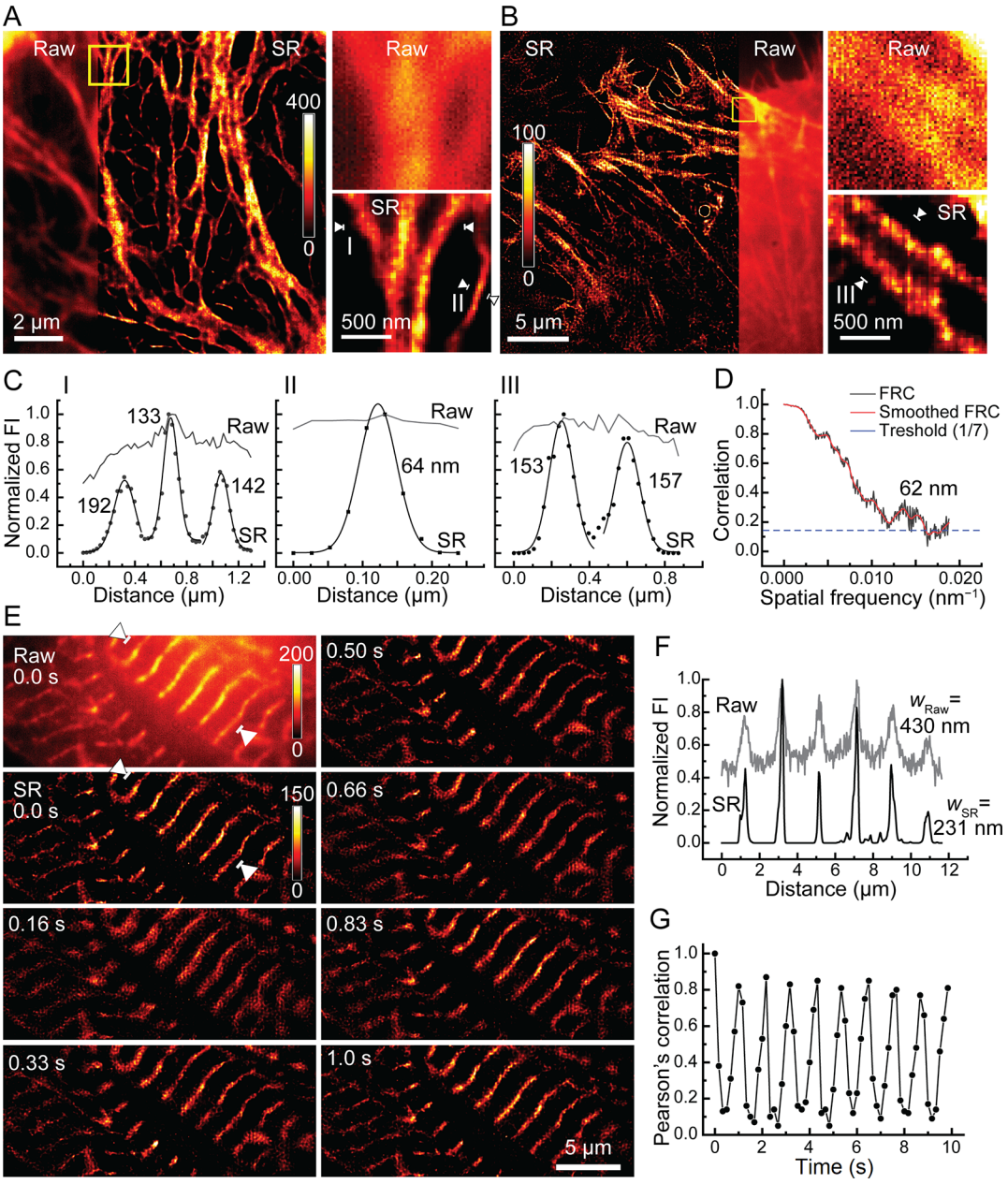

Figure 4. SR imaging of rsZACRO fusion proteins in live HeLa cells and human iPSC-derived cardiomyocyte by SPoD-OnSPAN. (A,B) Raw and SR images of (A) vimentin intermediate filaments and (B) actin filaments in live HeLa cells. The right panels in (A,B) display magnified views of the areas enclosed by squares in the left panels. The raw image is an average of over 20 frames taken within 10 s during SPoD-OnSPAN observation. The rotation speed of the quarter waveplate is 6 rpm. SR images were generated from these frames using L_p-regularized maximum likelihood estimation with parameters p = 1.1, λ_g = 0.1, and λ_b = 5.0. Irradiation power densities were 2.5 W/cm^2 at 561 nm and 10 mW/cm^2 at 458 nm. (C) Line profiles of fluorescence intensity along the line segments indicated by arrows in (A,B). Profiles from raw (gray) and SR (black) images are shown. Gaussian distribution functions fitted to the data points analyze these profiles, with values indicating FWHM (nm) of the peaks. (D) FRC analysis of SR images to evaluate the lateral spatial resolution, with two SR images from the data set in (A) used for this analysis. A lateral spatial resolution of 62 nm was determined at a spatial frequency where a correlation value reached a threshold of 1/7. (E) Raw and a time series of SR images of Z-disc in a live human iPSC-derived cardiomyocyte expressing β-tubulin-rsZACRO. The raw image is an average of 10 frames taken in 0.16 s during SPoD-OnSPAN observation. The rotation speed of the quarter waveplate was 180 rpm. SR images were generated using L_p-regularized maximum likelihood estimation with parameters of p = 1.1, λ_g = 0.1, and λ_b = 5.0. Irradiation power densities were 28.2 W/cm^2 at 561 and 100 mW/cm^2 at 458 nm. (F) Line profiles of fluorescence intensity along the line segments indicated by the arrows in (E). Profiles from raw (gray) and SR (black) images show average spacing between two adjacent Z-discs of 1.93 μm (n = 5). w_{raw} and w_{SR} indicate average FWHM (nm) in raw and SR images, respectively (n = 6). (G) Colocalization analysis of SR images in (E) using Pearson's correlation coefficient to compare the SR image at 0 s with one at each subsequent time point. FI stands for fluorescence intensity. The color scale bars are linear and normalized to the maximum intensity value (in arbitrary unit) of each 32 bit image.

with genes encoding fusion proteins consisting of miRFP670-nano,[52] the PH domain, and either HyperNova, rsZACRO, mCherry, or EGFP (miRFP670nano-PH-HyperNova, miRFP670nano-PH rsZACRO, miRFP670nano-PH mCherry,

https://doi.org/10.1021/acsnano.4c16847
ACS Nano 2025, 19, 7188−7201

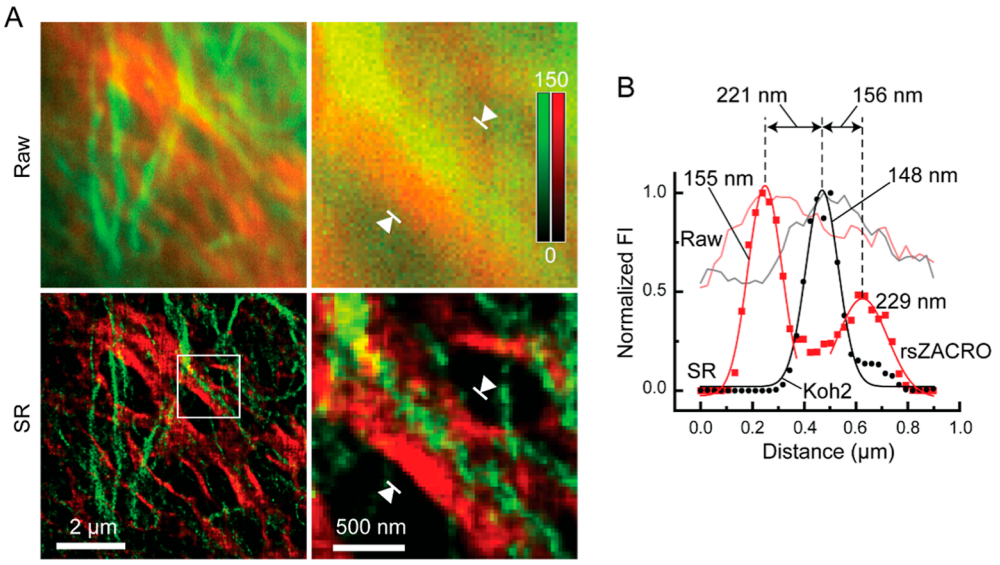

Figure 5. Two-color SR imaging of Kohinoor2.0 and rsZACRO in a live HeLa cell with single irradiation light for off-switching. (A) Merged raw (upper panels) and SR (lower panels) images of HeLa cell expressing LifeAct-Kohinoor2.0 (green channel) and vimentin-rsZACRO (red channel). Right panels show enlarged views of areas enclosed by square in the left SR image. The raw image compiles an average of 20 individual frames captured over 20 s during SPoD-OnSPAN observation. The rotation speed of the quarter waveplate was 3 rpm. SR images were reconstructed from these frames using L_p-regularized maximum likelihood estimation, with parameters set at p = 1.1, λ_g = 0.1, and λ_b = 5.0. Irradiation power densities were 0.69 W/cm^2 at 405, 1.2 W/cm^2 at 488, and 31.5 W/cm^2 at 561 nm. (B) Line profiles of fluorescence intensity along the arrows in (A), with solid lines indicating Gaussian distribution fits to the SR data. Values represent the FWHM (nm) in nanometers peaks in the green (Kohinoor2.0) and red (rsZACRO) channels. Koh2 stands for Kohinoor2.0 and FI for fluorescence intensity. The color scale bars are linear and normalized to the maximum intensity value (in arbitrary unit) of each 32 bit image.

or miRFP670nano-PH-EGFP), and monitored their localization using miRFP670nano with a confocal microscope. After irradiating the cells with 554 nm light, we observed significant dissociation of miRFP670nano-PH-HyperNova from the cell membrane, evidenced by a marked decrease in miRFP670nano fluorescence intensity on the cell membrane. In contrast, there was minimal dissociation of miRFP670nano-PH-EGFP (Supporting Information Figure S8B), consistent with the previous reports.[39,51] Notably, the dissociation of miRFP670-nano-PH-rsZACRO was considerably less pronounced than that observed with miRFP670nano-PH-HyperNova and miRFP670nano-PH-mCherry, highlighting the suitability of rsZACRO as a fluorescent tag for live cell imaging.

SR Imaging of rsZACRO Fusion Proteins in Live HeLa Cells and Human iPSC-Derived Cardiomyocyte by SPoD-OnSPAN. We conducted SR imaging of HeLa cells expressing vimentin-rsZACRO and those expressing rsZACRO fused with actin-binding polypeptide LifeAct (LifeAct-rsZACRO) using SPoD-OnSPAN technique,[22,23] which exploits the photoswitching properties of fluorescent proteins to enhance spatial resolution. Figure 4A,B show wide-field raw images of vimentin-rsZACRO and LifeAct-rsZACRO, respectively, alongside their corresponding SPoD-OnSPAN images, where the improved spatial resolution is evident. Furthermore, line profiles of fluorescence intensities across vimentin intermediate filaments and actin filaments, as indicated by the line segments in Figure 4A,B (bottom right images), distinctly reveal three and two peaks, respectively (black curves in Figure 4CI,III). In contrast, these peaks are less distinct in the line profiles (gray curves in Figure 4CI,III) from the wide-field fluorescence images (upper right images in Figure 4A,B). The full width at half-maximum (FWHM) of the cross-section of the rsZACRO-labeled vimentin intermediate filament, as profiled, was 64 nm (Figure 4CII), closely matching the spatial resolution of 62 nm determined by Fourier ring correlation (FRC) analysis (Figure 4D).[53] For reference, a study using scanning transmission electron microscopy reported that the diameter of vimentin intermediate filaments is approximately 30 nm.[54] In addition, we conducted a comparative study of SR images of vimentin-rsZACRO and vimentin-rsCherry expressed in HeLa cells (Supporting Information Figure S9A). We conducted SPoD-OnSPAN observations followed by SPoD observations, which did not involve photoswitching, in the same field of view to calculate and compare the reconstructed SR images of vimentin-rsZACRO and vimentin-rsCherry (Supporting Information Figure S9A). FRC data from SPoD-OnSPAN (Supporting Information Figure S9B) demonstrated higher correlation values in the high spatial frequency range of 0.01−0.019 nm^{-1} (equivalent to 100−53 nm in space domain) than those from SPoD, highlighting the enhanced spatial resolution achieved by incorporating fluorescent protein photoswitching in SPoD-OnSPAN observations (Supporting Information Figure S9C). Furthermore, FRC analysis showed that the correlation values in the spatial frequency range of 0.01−0.019 nm^{-1} for vimentin-rsZACRO using SPoD-OnSPAN were significantly higher than those for vimentin-rsCherry, while the correlation values in the same frequency range from the SPoD images were comparable between rsZACRO and rsCherry, and close to zero (Supporting Information Figure S9B,C). Therefore, these results indicate that the reconstructed image of vimentin-rsZACRO by SPoD-OnSPAN retained more detailed features than that of vimentin-rsCherry under the same observation conditions. As previously discussed, (see Properties of rsZACRO in live mammalian cells), the off-switching kinetics and on/off contrast of rsZACRO are 5.3 and 1.5 times higher, respectively, than those of rsCherry. These photoswitching properties likely contribute to the enhanced spatial resolution

https://doi.org/10.1021/acsnano.4c16847
ACS Nano 2025, 19, 7188−7201

in SPoD-OnSPAN imaging with rsZACRO compared to rsCherry, aligning with the operational principle of SPoD-OnSPAN.[25,26] Since the observation conditions were not optimized for the SPoD-OnSPAN imaging with rsCherry, it might be possible to achieve a spatial resolution comparable to SR imaging with rsZACRO by increasing the power density of the illumination light. However, this would require a higher power density for off-switching than that used in SR imaging with rsZACRO, leading to increased phototoxicity in living samples during observation.

We also conducted time-lapse SR imaging of a cardiomyocyte derived from human induced pluripotent stem cells (iPSCs) expressing β-tubulin fused with rsZACRO (β-tubulin-rsZACRO) using SPoD-OnSPAN technique. Figure 4E shows a raw image alongside a time series of sequentially captured SR images, revealing that the periodically aligned structure of β-tubulin-rsZACRO localizes on the Z-discs of sarcomeres.[55,56] Line profiles of fluorescence intensities across Z-discs, as indicated in Figure 4E (raw and SR images at 0 s), demonstrated average FWHM's of 231 and 430 nm for SR and raw image, respectively, again underscoring the enhanced spatial resolution achieved through SPoD-OnSPAN imaging (Figure 4F). The average distance measured between adjacent Z-discs was 1.93 μm (Figure 4F), consistent with previous reports of sarcomere length ranging from 1.7 to 2.0 μm.[57,58] In this time-lapse imaging study, we captured reconstructed SR images at a frame rate of 6 Hz for 10 s, and successfully tracked the movement of Z-discs in beating cardiomyocyte at approximately 1.1 s intervals (Figure 4E). Cardiomyocyte contractions were analyzed through colocalization analysis of SR images captured at 0 s and subsequent time points (Figure 4G). Such time lapse SR analysis of detailed structure could be instrumental in identifying cellular abnormalities associated with cardiac diseases, such as hypertrophic cardiomyopathy.[56] Moreover, high-resolution time-lapse observation of the sarcomere structure could provide more detailed assessments of the maturation of human iPSC-derived cardiomyocytes.

Two-Color SR Imaging of rsZACRO and Kohinoor2.0 in a Live HeLa Cell with Single Irradiation Light for Off-Switching. Multiplex labeling of cells with rsZACRO and Kohinoor2.0, a green p-rsFP,[27] facilitates two-color SR imaging. To simplify the optical setup for two-color SR imaging, we used a 405 nm laser beam for off-switching of both rsZACRO and Kohinoor2.0 in the SPoD-OnSPAN microscope (Supporting Information Figure S10), having confirmed that rsZACRO also underwent off-switching with a 405 nm beam (Supporting Information Figure S11A,B and Table S1). Consequently, we conducted two-color SPoD-OnSPAN observations of vimentin-rsZACRO (red channel) and Life-Act-Kohinoor2.0 (green channel) in HeLa cells. Figure 5A shows merged wide-field and SPoD-OnSPAN images of a cell from the two channels, highlighting how vimentin intermediate filaments (in red) and actin filaments (in green) are more distinctly delineated in the SR images than in the wide-field images. In fact, the line profiles of fluorescence intensities marked by white arrows in Figure 5A clearly reveal a single peak in the green channel between two peaks in the red channel, which are difficult to resolve in the wide-field raw image (Figure 5B). Here, we note that for these observations, we meticulously adjusted the optical alignment of the green and red fluorescence emission channels (Supporting Information Figure S12A) and validated this alignment through two-color SPoD-OnSPAN observations of vimentin-rsZACRO and vimentin-Kohinoor2.0 in HeLa cells, demonstrating highly precise colocalization between the two channels (Supporting Information Figure S12B). The line profiles of fluorescence intensities across vimentin intermediate filaments, indicated by arrows in Supporting Information Figure S12C, reveal an overlap of the two-color channels (Supporting Information Figure S12D-1,2). However, a slight misalignment was also noticeable, potentially due to the time lag between capturing the two channels or variation in the spatial distribution of vimentin-Kohinoor2.0 and vimentin-rsZACRO (Supporting Information Figure S12D-3). Additionally, the line profiles indicated improved spatial resolution in the SR images (dots and solid curves in Supporting Information Figure S12D) compared to the raw images (light lines in Supporting Information Figure S12D), achieving spatial resolutions of 57 and 65 nm for the green and red channels, respectively, as measured by the FWHM (Supporting Information Figure S12D). Furthermore, we verified that the fluorescence crosstalk between the green and red channels was negligibly small (Supporting Information Figure S13A,B). Thus, in the two-color SR imaging using a single light for off-switching, we successfully visualized the vimentin intermediate filament and actin filament networks at a resolution surpassing the diffraction limit of light in living HeLa cells.

CONCLUSION

Although several p-rsRFPs have been reported to date, conventional p-rsRFPs typically lack properties such as high fluorescence brightness, efficient photoswitching, and effective performance as fusion tags for SR imaging, thereby limiting the color palette options for SR imaging techniques that utilize p-rsFPs. In this study, we developed rsZACRO, a p-rsRFP that exhibited fluorescence 3.0 times brighter, off-switching 5.3 times faster, and on/off contrast 1.5 times higher in HeLa cells compared to rsCherry, a conventional p-rsRFP. Employing rsZACRO with the SPoD-OnSPAN technique, we demonstrated SR imaging of rsZACRO fusion proteins in live cells, showcasing its red fluorescence and confirming an improvement in spatial resolution over that obtained using rsCherry. Furthermore, using rsZACRO and Kohinoor2.0, we achieved two-color SR imaging of vimentin intermediate filaments and actin filaments in HeLa cells visualizing these structures at the nanometer scale. In these observations, we utilized a single 405 nm laser beam to off-switch both rsZACRO and Kohinoor2.0 in the SPoD-OnSPAN microscope, capitalizing on the enhanced properties of rsZACRO.

rsZACRO is expected to broaden the color palettes available for SR imaging with p-rsFPs. Although this study focused on using rsZACRO in SPoD-OnSPAN imaging, we anticipate its effectiveness in other SR techniques involving p-rsFPs, such as RESOLFT[28,29] and NL-SIM.[30] Furthermore, rsZACRO allowed for multicolor SR and highly biocompatible SR imaging, utilizing longer wavelengths for excitation and off-switching compared to conventional green p-rsFPs. Beyond SR imaging, rsZACRO also offers a red fluorescence tagging option for techniques involving rsFPs, such as out-of-phase imaging after optical modulation[11,59] and temporally multiplexed imaging.[13] However, the photostability of rsZACRO may still be suboptimal for certain applications including long-term SR imaging (Supporting Information Figure S6A). In the future, further enhancements to rsZACRO will facilitate biocompatible, long-term, and multicolor SR imaging, enabling the simultaneous tracking of minute dynamic details in diverse

https://doi.org/10.1021/acsnano.4c16847
ACS Nano 2025, 19, 7188−7201

cellular components such as intracellular organelles and proteins.

MATERIALS AND METHODS

Mutagenesis and Measuring the Fluorescence Intensity of *E. coli* Colonies for Screening. For the site-directed mutagenesis, we amplified the pRSET$_B$ vector harboring the HyperNova gene using primers that incorporated a random nucleotide (NNK) or a specific mutation, utilizing PCR with KOD-Plus DNA polymerase (Toyobo). For screening, we incubated *E. coli* JM109(DE3) cells, transformed with the resultant cDNA on an 88 mm LB agar plate at 37 °C for 16 h, followed by a further incubation at room temperature for 1 day. We measured the fluorescence intensity of these *E. coli* colonies using an in-house-built illumination system consisting of a CCD camera (01-QIClick-F-M12; QImaging), a bandpass filter (FF01-641/75-25, Semlock), and an LED light source (SPECTRA X Light Engine; Lumencor) (Supporting Information Figure S1). Photoswitching was monitored by sequentially irradiating the colonies with light at 542 and 438 nm for on-switching and off-switching, respectively. We analyzed the data using ImageJ Fiji software.[60]

Gene Construction for Cell Expression Vectors. To study the photoswitching of p-rsRFPs (asFP595-T70A/A148S, rsCherry, and rsZACRO) in mammalian cells, we amplified the rsZACRO gene within the pRSET$_B$ vector using PCR primers designed with *Bam*HI and *Eco*RI restriction sites. This PCR product was used to replace the Kohinoor2.0 gene in the mammalian expression vector pcDNA3, creating Vimentin-p-rsRFPs (Vimentin-p-rsRFPs/pcDNA3).[27] To compare brightness in mammalian cells, we substituted the mCherry gene with an amplified EGFP gene using *Hin*dIII and *Bam*HI restriction sites, and replaced the Kohinoor2.0 gene with amplified p-rsRFPs using NheI and NotI restriction sites in the mCherry-P2A-Kohinoor2.0/pcDNA3 vector, generating EGFP-P2A-p-rsRFPs/pcDNA3.[27] Evaluating rsZACRO's performance as a fusion protein or fluorescent tag, we substituted the Kohinoor2.0 gene with the amplified rsZACRO at *Bam*HI and *Eco*RI sites in pcDNA3, resulting in rsZACRO/pcDNA3, Lifeact-rsZACRO/pcDNA3, and Zyxin-rsZACRO/pcDNA3. Additionally, we achieved replacements between *Hin*dIII and *Eco*RI to yield rsZACRO-Fibrillarin and rsZACRO-H2B/pcDNA3, and used *Eco*RI and NotI to create β-tubulin-rsZACRO/pcDNA3.[27] We amplified the Keratin,[38] EB3 (from HeLa cell cDNA library), Cox8A (Addgene #101129), and Sec-61β[61] genes by PCR using primers containing *Hin*dIII and *Eco*RI, *Hin*dIII and *Bam*HI, *Kpn*I and *Eco*RI, and *Eco*RI and XhoI restriction sites, respectively. The restricted products were subsequently used to replace genes previously fused with rsZACRO, resulting in the creation of Keratin-rsZACRO, EB3-rsZACRO, Cox8A-rsZACRO, and rsZACRO-Sec61β constructs. To construct rsZACRO-CAAX/pcDNA3, we amplified the CAAX gene, which includes the 20 *C*-terminal amino acids of K-Ras, using primers with *Eco*RI and XhoI restriction sites. The PCR product was then used to replace a gene fused with rsZACRO. To investigate phototoxicity in mammalian cells, we amplified miRFP670nano, PHdomain (Addgene #21179), and fluorescent proteins (FPs) such as EGFP, mCherry, HyperNova, and rsZACRO using primers containing *Bam*HI and *Bgl*II, *Bgl*II and *Eco*RI, and *Eco*RI and XhoI restriction sites, respectively. We then ligated these amplified genes using the respective restriction sites to generate miRFP670nano-PHdomain-FPs/pcDNA3. In our study of maturation kinetics, we replaced the Kohinoor2.0 gene with amplified red fluorescent proteins (RFPs) such as HyperNova, asFP595-T70A/A148S, rsCherry, and rsZACRO at the *Bgl*II and *Eco*RI restriction sites of the pBAD vector.[27]

Protein Purification. We expressed fluorescent proteins tagged with a 6 × His-tag at the *N*-terminus in *E. coli* JM109(DE3) at 23 °C for approximately 70 h in LB medium supplemented with 0.1 mg/mL carbenicillin. After harvesting, we resuspended the cells in PBS buffer containing a protease inhibitor (cOmplete EDTA-free; Merck), and lysed them using a French press (French Press G-M Model 11; Glen Mills). Subsequently, we purified the fluorescent proteins from the supernatant through affinity chromatography on a Ni-NTA agarose (QIAGEN) column, followed by gel filtration on a PD-10 column (GE Healthcare BioSciences) preequilibrated with 20 mM HEPES-NaOH (pH 7.5).

***In Vitro* Characterization.** We measured the absorption spectrum, fluorescence excitation and emission spectra, and fluorescence quantum yield of purified proteins using a U-3900 spectrophotometer (Hitachi High-Tech Science), a F-7000 fluorescence spectrophotometer (Hitachi High-Tech Science), and a Quantarus-QY spectrophotometer (C11347-01; Hamamatsu Photonics), respectively. To determine the concentration of purified proteins and subsequently calculate their molar extinction coefficients, we employed the bicinchoninic acid (BCA) assay (Protein Assay BCA Kit; Wako). We measured the pH-dependent absorption spectra of these proteins, by mixing 6 μL of protein solution with 394 μL of a buffer solution. For pH values from 2.5 to 8.5, we prepared a buffer solution containing 30 mM trisodium citrate and 30 mM sodium tetraborate, adjusting the pH with HCl. For pH values from 9.0 to 12.0, we used a buffer of 30 mM CHES (*N*-cyclohexyl-2-aminoethanesulfonic acid) and 30 mM CAPS (*N*-cyclohexyl-3-aminopropanesulfonic acid), both from Dojindo, adjusting the pH with NaOH. Before measurements, we incubated the purified rsZACRO solution in the dark for over 15 min. We exposed rsCherry and asFP595-T70A/A148S to light at 542 nm (110 mW/cm^2) for 15 min to transition them to the on-state. For the off-switching of rsZACRO, we irradiated the solutions with light at 432 nm (80 mW/cm^2) for 1 min.

Fitting pH Titration Curve. Using the four-state model illustrated in Supporting Information Figure S4B, we defined the equilibrium constants for chromophore conformation changes, L_H, K_1, and K_2, as follows

$$L_H = \frac{[C^- - XH]}{[C^- - X^-]x},\ K_1 = \frac{[CH - X^-]}{[C^- - X^-]x},\ \text{and}\ K_2 = \frac{[CH - XH]}{[C^- - XH]x} \tag{1}$$

where $x = [H^+]$ and $K_1 > K_2$. Therefore, the model function simulating the apparent absorbance, A_{model}, is derived as follows

$$\begin{aligned} A_{model} &= A_{C^-}\frac{[C^- - X^-] + [C^- - XH]}{[C^- - X^-] + [C^- - XH] + [CH - X^-] + [CH - XH]} \\ &\quad + A_{CH}\frac{[CH - X^-] + [CH - XH]}{[C^- - X^-] + [C^- - XH] + [CH - X^-] + [CH - XH]} \\ &= A_{C^-}\frac{1 + L_H x}{1 + (L_H + K_1)x + L_H K_2 x^2} + A_{CH}\frac{K_1 x + L_H K_2 x^2}{1 + (L_H + K_1)x + L_H K_2 x^2} \end{aligned} \tag{2}$$

where A_{C-} and A_{CH} represent the absorbances values at a 100% mole fraction for the protonated (C^-) and protonated (CH) states of the chromophores. We used the A_{model} to fit the measured data to determine the optimal values of the equilibrium constants using OriginPro 2021 software (OriginLab).

Measurement of Oxygen-dependent Maturation Speed of FPs. We cultured *E. coli* JM109(DE3) cells transformed with a pBAD vector harboring the genes for rsZACRO, HyperNova, rsCherry, or asFP595-T70A/A148S in 10 mL of LB medium supplemented with 0.1 mg/mL carbenicillin at 37 °C. Once the optical density at 595 nm of the culture exceeded 0.5, we added arabinose to a final concentration 0.4% w/v to induce protein expression and continued to incubate for over 4 h at 37 °C under anaerobic conditions using AnaeroPack (Mitsubishi Gas Chemical). Cells were then harvested by centrifugation at 7300×*g* for 3 min at 4 °C, resuspended in PBS containing a protease inhibitor (cOmplete; Merck), and lysed by

https://doi.org/10.1021/acsnano.4c16847
ACS Nano 2025, 19, 7188−7201

ultrasonication on ice. The mixture lysate was centrifuged at 20,600×*g* for 3 min at 4 °C to separate the supernatant. The fluorescence intensity of the supernatant was monitored every 3 min at 37 °C under air-saturated conditions using an F-7000 fluorescence spectrophotometer (Hitachi High-Tech Science). The half-time of chromophore maturation was calculated by fitting an asymptotic exponential function to the fluorescence data using OriginPro 2021 (OriginLab).

Measurement of Phototoxicity in *E. coli*. To evaluate the phototoxicity of fluorescent proteins (FPs) in *E. coli*, we cultured *E. coli* JM109(DE3) transformed with a pRSET$_B$ vector containing rsZACRO, HyperNova, EGFP, or mCherry at 23 °C for 3 days in LB medium supplemented with 0.1 mg/mL carbenicillin. Subsequently, the cells were diluted in PBS and split into two groups. One group was irradiated with light at 542 nm (100 mW/cm^2) using an LED light source (SPECTRA X Light Engine; Lumencor) for 30 min, while the other was kept in the dark. After exposure, both groups were incubated on LB agar plates at 37 °C for over 18 h. We then counted the number of viable colonies. The survival rate was determined by comparing the ratio of colonies that survived light exposure to those incubated in the dark.

Mammalian Cell Culture and Transfection. HeLa cells were cultured in Dulbecco's modified Eagle's medium (D-MEM (low glucose), 041-29775, Wako) supplemented with 10% (v/v) fetal bovine serum. We transfected HeLa cells that had been transferred to a 35 mm glass-bottom dish, using polyethylenimine (PEI Max 40K; Polysciences) according to the manufacturer's instructions. Cardiomyocytes were differentiated from human iPSCs through monolayer culture by modulating Wnt signaling, as previously described,[62,63] and cryopreserved on day 15 of differentiation. For reculturing from frozen stock, cells were initially cultured for 24 h on Matrigel-coated dishes in RPMI-1640 (189-02145, FUJIFILM Wako) supplemented with B27 (17504044, Thermo Fisher Scientific) and penicillin−streptomycin, thereafter, referred to as RPMI/B27 medium, and 10% KnockOut Serum Replacement (10828010, Thermo Fisher Scientific). Afterward, the medium was changed to RPMI/B27 medium. On day 19 of differentiation, the cells were passaged using TrypLE Select (A1285901, Thermo Fisher Scientific) onto Matrigel-coated glass-bottom dishes. For the first 24 h after passage, RPMI/B27 medium with 10% KnockOut Serum Replacement was used, and after that, the cells were cultured in RPMI/B27 medium. Human iPSC derived cardiomyocytes that had been transferred to a 35 mm glass-bottom dish were transfected using VisFect transfection Reagent (E498A; Promega) following the manufacturer's instructions. More than 36 h after gene transfection of HeLa cells or cardiomyocytes, we replaced the medium with DMEM/F12 (11039021; Thermo Fisher Scientific) supplemented with 10% (v/v) fetal bovine serum (S1780; Biowest, Riverside), and then performed observations.

Cell Imaging and Measurement of Phototoxicity in HeLa Cells. We observed HeLa cells expressing vimentin-p-rsRFP variants (rsZACRO, rsCherry, or asFP595-T70A/A148S), EGFP-P2A-p-rsRFP, rsZACRO fused with various proteins or localization tags, and miRFP670nano-PHdomain-FPs (rsZACRO, HyperNova, mCherry, or EGFP), using a Nikon Ti-2 inverted microscope equipped with a Dragonfly 200 confocal unit (Andor Technology), a CFI Plan Apochromat λ 100× Oil objective (Numerical Aperture 1.40; Nikon), and a Tokai Hit stage-top incubator. We used 488, 561, and 630 nm laser lines to excite EGFP, p-rsRFPs and HyperNova, and miRFP670nano, respectively. Fluorescence was captured using TR-DFLY-F521-038, TR-DFLY-F600-050, and TR-DFLY-F700-075 bandpass filters (Andor Technology) for EGFP, p-rsRFPs/HyperNova, and miRFP670nano, respectively, with an iXon Ultra EMCCD camera (Andor Technology). To assess the phototoxicity of rsZACRO in cells expressing miRFP670nano-PH-FPs, we exposed them to 554 nm light at 1.4 W/cm^2 for 30 s using a Niji LED light source (Bluebox Optics). The localization of the pH domain was quantified by analyzing the intensity of miRFP670nano fluorescence images processed with a first derivative filter in ImageJ Fiji software.

Measurement of Photoswitching, Photobleaching, and Photoswitching Fatigue. For our studies on photoswitching, photobleaching, and photoswitching fatigue, we employed an Olympus IX83 inverted microscope, equipped with a 100× oil immersion objective (UPLXAPO100XO, NA 1.45; Olympus), a Z-drift compensator (IX3-ZDC2; Olympus), an ultrasonic motorized stage (IX3-SSU; Olympus), and a Tokai Hit stage-top incubator. Fluorescence excitation and switching were managed with a 561 nm laser (Sapphire; Coherent) for excitation and on-switching, and 405 nm laser (OBIS 405LX-100-HS-WM; Coherent) and 458 nm laser (Sapphire; Coherent) for off-switching. Captured fluorescence was filtered through a FF01-647/57 bandpass filter (Semrock) and imaged with an ORCA-Flash4.0 V2 complementary metal-oxide-semiconductor (CMOS) camera (Hamamatsu Photonics). ImageJ Fiji software was utilized for image analysis. To determine the photoswitching kinetic rate constants, we analyzed fluorescence intensity time trajectories using pseudo-first order kinetics, following previously established methods.[25] The equilibrium fluorescence intensity F_{ON+OFF} of a p-rsFP, when both on-switching/excitation and off-switching lights are simultaneously irradiated, is given by

$$F_{ON+OFF} = \frac{F_{ON}k_{ON} + F_{OFF}k_{OFF}}{k_{ON} + k_{OFF}} \quad (3)$$

where F_{ON} and F_{OFF} represent the fluorescence intensities of the on and off states, respectively, and k_{ON} and k_{OFF} are the rate constants, for on- and off-switching under specific light power densities.[25,27] The on/off contrast as detailed in Supporting Information Table S1, was computed from eq 3, as follows

$$\frac{F_{ON}}{F_{OFF}} = \frac{F_{ON}k_{OFF}}{F_{ON+OFF}(k_{ON} + k_{OFF}) - F_{ON}k_{ON}} \quad (4)$$

These analyses were conducted using OriginPro 2021 (OriginLab).

Superresolution Imaging. For superresolution (SR) imaging, we utilized the SPoD-OnSPAN technique.[25,26] The SPoD-OnSPAN technique is based on a wide-field epi-fluorescence microscopy configuration. In SPoD observation, linearly polarized illumination light with a rotating polarization plane was used to excite the fluorophore. The fluorescence intensity from a fixed fluorophore is proportional to $\cos^2(\omega t - \theta)$, where ω, t and θ represent the angular velocity of rotation, time, and phase shift dependent on the fluorophore's orientation, respectively, resulting in fluorescence modulation. Furthermore, in SPoD-OnSPAN observation, linearly polarized off-switching light was used in addition to excitation and on-switching light, enabling a photoswitching fluorescent probe to undergo cycles of on- and off-switching, which enhanced the modulation amplitude. A superresolved image was reconstructed using L_p-regularized maximum-likelihood calculations from the observed data set containing fluorescence modulation information.[25] For SPoD-OnSPAN observation, we used an IX83 microscope equipped with a UPLXAPO100XO oil-immersion objective (100× magnification, NA = 1.45; Olympus). We used a 561 nm laser (Sapphire 561-150 CW CDRH; Coherent) for excitation and on-switching of rsZACRO, and a 458 nm laser (Sapphire 458−75 CW CDR; Coherent) for off-switching p-rsRFPs. For two-color SR imaging, we utilized the same 561 nm laser for rsZACRO, a 488 nm laser (PC14584; Spectra-Physics) for Kohinoor2.0, with a 405 nm laser (OBIS 405LX-100-HS-WM; Coherent) for simultaneous off-switching. We captured fluorescence using two CMOS cameras (ORCA-Flash4.0 V2 C11440−22CU; Hamamatsu Photonics) through a dual view optics system (W-View Gemini-2c A12801-10; Hamamatsu Photonics), utilizing FF01-647/57 and FF01-525/45-25 bandpass filters (Semrock) for rsZACRO and Kohinoor2.0, respectively, dichroic mirrors (ZT405-488/568rpc-UF1, 26 × 38; Chroma and FF560-FDi02-t3-25 × 36; Semrock) facilitated separation of green and red fluorescence. Image reconstruction was performed using a custom C++ program developed in our previous study,[25] compiled with Intel C/C++ compiler (ver. 19.0, Intel). We assessed the spatial resolution of SR images by Fourier ring correlation (FRC) analysis[53] using an ImageJ plugin (available at https://github.com/BIOP/ijp-frc). Colocalization analysis was executed using ImageJ Fiji software.

https://doi.org/10.1021/acsnano.4c16847
ACS Nano 2025, 19, 7188−7201

ASSOCIATED CONTENT

Supporting Information

The Supporting Information is available free of charge at https://pubs.acs.org/doi/10.1021/acsnano.4c16847.

Figure S1. Imaging of *E. coli* colonies expressing fluorescent protein. Figure S2. Amino acid sequences of HyperNova and rsZACRO. Figure S3. Oxygen dependent chromophore maturation of rsZACRO at 37 °C. Figure S4. pH dependent absorbance spectra and an equilibrium model describing the pH dependence. Figure S5. On-switching of rsZACRO in HeLa cells. Figure S6. Photobeaching and photoswitching fatigue of rsZACRO in HeLa cells. Figure S7. Confocal images of the localization of asFP595-T70A/A148S in HeLa cells. Figure S8. Phototoxicity of rsZACRO in *E. coli* and in mammalian cells. Figure S9. Comparison of spatial resolution in SPoD-OnSPAN imaging between rsZACRO and rsCherry and between SPoD-OnSPAN and SPoD imaging. Figure S10. SPoD-OnSPAN microscope for two color SR imaging. Figure S11. Photoswitching of rsZACRO by 405 nm. Figure S12. Co-localization in two color SPoD-OnSPAN observation setup. Figure S13. Fluorescence crosstalk in two-color SPoD-OnSPAN observation setup (PDF)

AUTHOR INFORMATION

Corresponding Author

Takeharu Nagai − *SANKEN (The Institute of Scientific and Industrial Research), Osaka University, Ibaraki, Osaka 567-0047, Japan; Graduate School of Frontier Biosciences and Transdimensional Life Imaging Division, Institute for Open and Transdisciplinary Research Initiatives, Osaka University, Suita, Osaka 565-0871, Japan; Research Institute for Electronic Science, Hokkaido University, Sapporo, Hokkaido 001-0020, Japan;* orcid.org/0000-0003-2650-9895; Email: ng1@sanken.osaka-u.ac.jp

Authors

Ryohei Ozaki-Noma − *SANKEN (The Institute of Scientific and Industrial Research), Osaka University, Ibaraki, Osaka 567-0047, Japan; Graduate School of Frontier Biosciences, Osaka University, Suita, Osaka 565-0871, Japan*

Tetsuichi Wazawa − *SANKEN (The Institute of Scientific and Industrial Research), Osaka University, Ibaraki, Osaka 567-0047, Japan;* orcid.org/0000-0002-4171-585X

Taishi Kakizuka − *SANKEN (The Institute of Scientific and Industrial Research), Osaka University, Ibaraki, Osaka 567-0047, Japan; Transdimensional Life Imaging Division, Institute for Open and Transdisciplinary Research Initiatives, Osaka University, Suita, Osaka 565-0871, Japan*

Hisashi Shidara − *Graduate School of Medicine, Mie University, Tsu, Mie 514-8507, Japan*

Kiwamu Takemoto − *Graduate School of Medicine, Mie University, Tsu, Mie 514-8507, Japan*

Complete contact information is available at: https://pubs.acs.org/10.1021/acsnano.4c16847

Author Contributions

T.N. conceived and coordinated the project. R.O.-N. designed the fluorescent protein. K.T., H.S. constructed HyperNova. R.O.-N., T.W., T.K., and T.N. designed the experiments. R.O.-N. performed experiments. R.O.-N., T.W., and T.N. analyzed the data. R.O.-N. and T.W. wrote the manuscript draft, and T.N. edited it.

Funding

This work was in part supported by a grant from Core Research for Evolutionary Science and Technology, Japan Science and Technology Agency (JPMJCR15N3 to T.N.), a Grant-in-Aid for Scientific Research on Innovative Areas "Singularity Biology (No. 8007)" (18H05408 and 18H05410 to T.N.), and Grant-in-Aid from The Japan Society for the Promotion of Science (21K19225 to T.N.; 22K04891 to T.W.; 23KJ1492 to R.O.-N.).

Notes

The authors declare no competing financial interest.

ACKNOWLEDGMENTS

We thank K. Sugiura for technical instructions and valuable discussion.

ABBREVIATIONS

rsFP, reversibly photoswitching fluorescent protein; p-rsFP, positive-type reversibly photoswitching fluorescent proteins; n-rsFP, negative-type reversibly photoswitching fluorescent proteins; p-rsRFP, positive-type reversibly photoswitching red fluorescent protein; SR, superresolution; RESOLFT, reversible saturable optical linear transitions; NL-SIM, nonlinear structured illumination microscopy; pcSOFI, photochromic stochastic optical fluctuation imaging; STED, stimulated emission depletion; SPoD-ExPAN, superresolution polarization demodulation/excitation polarization angle narrowing; SPoD-OnSAPN, superresolution polarization demodulation/on-state polarization angle narrowing; QY, fluorescence quantum yield; ESPT, excited-state proton transfer; PH, Plekstrin homology; ROS, reactive oxygen species; FWHM, full width at half-maximum; iPSC, induced pluripotent stem cells.

REFERENCES

(1) Zhou, X. X.; Lin, M. Z. Photoswitchable Fluorescent Proteins: Ten Years of Colorful Chemistry and Exciting Applications. *Curr. Opin. Chem. Biol.* **2013**, *17*, 682−690.

(2) Nifosì, R.; Storti, B.; Bizzarri, R. Reversibly Switchable Fluorescent Proteins: "the Fair Switch Project. *Riv. Nuovo Cimento.* **2024**, *47*, 91−178.

(3) Bourgeois, D.; Adam, V. Reversible Photoswitching in Fluorescent Proteins: A Mechanistic View. *IUBMB Life* **2012**, *64*, 482−491.

(4) Nienhaus, K.; Nienhaus, G. U. Chromophore Photophysics and Dynamics in Fluorescent Proteins of the GFP family. *J. Phys.: Condens. Matter* **2016**, *28*, 443001.

(5) Ando, R.; Mizuno, H.; Miyawaki, A. Regulated Fast Nucleocytoplasmic Shuttling Observed by Reversible Protein Highlighting. *Science* **2004**, *306*, 1370−1373.

(6) Zhou, X. X.; Chung, H. K.; Lam, A. J.; Lin, M. Z. Optical Control of Protein Activity by Fluorescent Protein Domains. *Science* **2012**, *338*, 810−814.

(7) Marriott, G.; Mao, S.; Sakata, T.; Ran, J.; Jackson, D. K.; Petchprayoon, C.; Gomez, T. J.; Warp, E.; Tulyathan, O.; Aaron, H. L.; Isacoff, E. Y.; Yan, Y. Optical Lock-in Detection Imaging Microscopy for Contrast-enhanced Imaging in Living Cells. *Proc. Natl. Acad. Sci. U.S.A.* **2008**, *105*, 17789−17794.

(8) Yan, Y.; Marriott, M. E.; Petchprayoon, C.; Marriott, G. Optical Switch Probes and Optical Lock-in Detection (OLID) Imaging Microscopy: High-contrast Fluorescence Imaging within Living Systems. *Biochem. J.* **2011**, *433*, 411−422.

(9) Quérard, J.; Le Saux, T.; Gautier, A.; Alcor, D.; Croquette, V.; Lemarchand, A.; Gosse, C.; Jullien, L. Kinetics of Reactive Modules Adds Discriminative Dimensions for Selective Cell Imaging. *ChemPhysChem* **2016**, *17*, 1396−1413.
(10) Valenta, H.; Hugelier, S.; Duwé, S.; Lo Gerfo, G.; Müller, M.; Dedecker, P.; Vandenberg, W. Separation of Spectrally Overlapping Fluorophores Using Intra-exposure Excitation Modulation. *Biophys. Rep* **2021**, *1*, 100026.
(11) Quérard, J.; Zhang, R.; Kelemen, Z.; Plamont, M.-A.; Xie, X.; Chouket, R.; Roemgens, I.; Korepina, Y.; Albright, S.; Ipendey, E.; Volovitch, M.; Sladitschek, H. L.; Neveu, P.; Gissot, L.; Gautier, A.; Faure, J.-D.; Croquette, V.; Le Saux, T.; Jullien, L. Resonant Out-of-phase Fluorescence Microscopy and Remote Imaging Overcome Spectral Limitations. *Nat. Commun.* **2017**, *8*, 969.
(12) Chouket, R.; Pellissier-Tanon, A.; Lahlou, A.; Zhang, R.; Kim, D.; Plamont, M.-A.; Zhang, M.; Zhang, X.; Xu, P.; Desprat, N.; Bourgeois, D.; Espagne, A.; Lemarchand, A.; Saux, T. L.; Jullien, L. Extra Kinetic Dimensions for Label Discrimination. *Nat. Commun.* **2022**, *13*, 1482.
(13) Qian, Y.; Celiker, O. T.; Wang, Z.; Guner-Ataman, B.; Boyden, E. S. Temporally Multiplexed Imaging of Dynamic Signaling Networks in Living Cells. *Cell* **2023**, *186*, 5656−5672.
(14) Subach, F. V.; Zhang, L.; Gadella, T. W.; Gurskaya, N. G.; Lukyanov, K. A.; Verkhusha, V. V. Red Fluorescent Protein with Reversibly Photoswitchable Absorbance for Photochromic FRET. *Chem. Biol.* **2010**, *17*, 745−755.
(15) Rainey, K. H.; Patterson, G. H. Photoswitching FRET to Monitor Protein−protein Interactions. *Proc. Natl. Acad. Sci. U.S.A.* **2019**, *116*, 864−873.
(16) Ojha, N.; Rainey, K. H.; Patterson, G. H. Imaging of Fluorescence Anisotropy during Photoswitching Provides a Simple Readout for Protein Self-association. *Nat. Commun.* **2020**, *11*, 21.
(17) Bierbuesse, F.; Bourges, A. C.; Gielen, V.; Mönkemöller, V.; Vandenberg, W.; Shen, Y.; Hofkens, J.; Vanden Berghe, P.; Campbell, R. E.; Moeyaert, B.; Dedecker, P. Absolute Measurement of Cellular Activities Using Photochromic Single-fluorophore Biosensors and Intermittent Quantification. *Nat. Commun.* **2022**, *13*, 1850.
(18) Volpato, A.; Ollech, D.; Alvelid, J.; Damenti, M.; Müller, B.; York, A. G.; Ingaramo, M.; Testa, I. Extending Fluorescence Anisotropy to Large Complexes Using Reversibly Switchable Proteins. *Nat. Biotechnol.* **2023**, *41*, 552−559.
(19) Hell, S. W. Far-Field Optical Nanoscopy. *Science* **2007**, *316*, 1153−1158.
(20) Hofmann, M.; Eggeling, C.; Jakobs, S.; Hell, S. W. Breaking the Diffraction Barrier in Fluorescence Microscopy at Low Light Intensities by Using Reversibly Photoswitchable Proteins. *Proc. Natl. Acad. Sci. U.S.A.* **2005**, *102*, 17565−17569.
(21) Jensen, N. A.; Jensen, I.; Kamper, M.; Jakobs, S. Reversibly Switchable Fluorescent Proteins for RESOLFT Nanoscopy. In *Nanoscale Photonic Imaging. Topics in Applied Physics*; Springer: Cham, 2020; Vol. *134*; pp 241−261..
(22) Rego, E. H.; Shao, L.; Macklin, J. J.; Winoto, L.; Johansson, G. A.; Kamps-Hughes, N.; Davidson, M. W.; Gustafsson, M. G. L. Nonlinear Structured-illumination Microscopy with a Photoswitchable Protein Reveals Cellular Structures at 50-nm Resolution. *Proc. Natl. Acad. Sci. U.S.A.* **2012**, *109*, E135−E143.
(23) Dedecker, P.; Mo, G. C. H.; Dertinger, T.; Zhang, J. Widely Accessible Method for Superresolution Fluorescence Imaging of Living Systems. *Proc. Natl. Acad. Sci. U.S.A.* **2012**, *109*, 10909−10914.
(24) Hafi, N.; Grunwald, M.; van den Heuvel, L. S.; Aspelmeier, T.; Chen, J.-H.; Zagrebelsky, M.; Schütte, O. M.; Steinem, C.; Korte, M.; Munk, A.; Walla, P. J. Fluorescence Nanoscopy by Polarization Modulation and Polarization Angle Narrowing. *Nat. Methods* **2014**, *11*, 579−584.
(25) Wazawa, T.; Arai, Y.; Kawahara, Y.; Takauchi, H.; Washio, T.; Nagai, T. Highly Biocompatible Super-resolution Fluorescence Imaging Using the Fast Photoswitching Fluorescent Protein Kohinoor and SPoD-ExPAN with L_p-regularized Image Reconstruction. *Microscopy* **2018**, *67*, 89−98.
(26) Wazawa, T.; Washio, T.; Nagai, T. Highly Biocompatible Super-resolution Imaging: SPoD-OnSPAN. Single Molecule Microscopy in Neurobiology. *Neuromethods* **2020**, *154*, 229−244.
(27) Wazawa, T.; Noma, R.; Uto, S.; Sugiura, K.; Washio, T.; Nagai, T. A Photoswitchable Fluorescent Protein for Hours-time-lapse and Sub-second-resolved Super-resolution Imaging. *Microscopy* **2021**, *70*, 340−352.
(28) Tiwari, D. K.; Arai, Y.; Yamanaka, M.; Matsuda, T.; Agetsuma, M.; Nakano, M.; Fujita, K.; Nagai, T. A Fast- and Positively Photoswitchable Fluorescent Protein for Ultralow-laser-power RESOLFT Nanoscopy. *Nat. Methods* **2015**, *12*, 515−518.
(29) Konen, T.; Stumpf, D.; Grotjohann, T.; Jansen, I.; Bossi, M.; Weber, M.; Jensen, N.; Hell, S. W.; Jakobs, S. The Positive Switching Fluorescent Protein Padron2 Enables Live-Cell Reversible Saturable Optical Linear Fluorescence Transitions (RESOLFT) Nanoscopy without Sequential Illumination Steps. *ACS Nano* **2021**, *15*, 9509−9521.
(30) Lu-Walther, H.-W.; Hou, W.; Kielhorn, M.; Arai, Y.; Nagai, T.; Kessels, M. M.; Qualmann, B.; Heintzmann, R. Nonlinear Structured Illumination Using a Fluorescent Protein Activating at the Readout Wavelength. *PLoS One* **2016**, *11*, No. e0165148.
(31) Shcherbakova, D. M.; Subach, O. M.; Verkhusha, V. V. Red Fluorescent Proteins: Advanced Imaging Applications and Future Design. *Angew. Chem., Int. Ed.* **2012**, *51*, 10724−10738.
(32) Stiel, A. C.; Andresen, M.; Bock, H.; Hilbert, M.; Schilde, J.; Schönle, A.; Eggeling, C.; Egner, A.; Hell, S. W.; Jakobs, S. Generation of Monomeric Reversibly Switchable Red Fluorescent Proteins for Far-Field Fluorescence Nanoscopy. *Biophys. J.* **2008**, *95*, 2989−2997.
(33) Lavoie-Cardinal, F.; Jensen, N. A.; Westphal, V.; Stiel, A. C.; Chmyrov, A.; Bierwagen, J.; Testa, I.; Jakobs, S.; Hell, S. W. Two-Color RESOLFT Nanoscopy with Green and Red Fluorescent Photochromic Proteins. *ChemPhysChem* **2014**, *15*, 655−663.
(34) Pennacchietti, F.; Serebrovskaya, E. O.; Faro, A. R.; Shemyakina, I. I.; Bozhanova, N. G.; Kotlobay, A. A.; Gurskaya, N. G.; Bodén, A.; Dreier, J.; Chudakov, D. M.; Lukyanov, K. A.; Verkhusha, V. V.; Mishin, A. S.; Testa, I. Fast Reversibly Photoswitching Red Fluorescent Proteins for Live-cell RESOLFT Nanoscopy. *Nat. Methods* **2018**, *15*, 601−604.
(35) Lukyanov, K. A.; Fradkov, A. F.; Gurskaya, N. G.; Matz, M. V.; Labas, Y. A.; Savitsky, A. P.; Markelov, M. L.; Zaraisky, A. G.; Zhao, X.; Fang, Y.; Tan, W.; Lukyanov, S. A. Natural Animal Coloration Can Be Determined by a Nonfluorescent Green Fluorescent Protein Homolog. *J. Biol. Chem.* **2000**, *275*, 25879−25882.
(36) Yanushevich, Y. G.; Staroverov, D. B.; Savitsky, A. P.; Fradkov, A. F.; Gurskaya, N. G.; Bulina, M. E.; Lukyanov, K. A.; Lukyanov, S. A. A Strategy for the Generation of Non-aggregating Mutants of Anthozoa Fluorescent Proteins. *FEBS Lett.* **2002**, *511*, 11−14.
(37) Shidara, H.; Shirai, T.; Ozaki-Noma, R.; Jitsuki, S.; Nagai, T.; Takemoto, K. Optical Inactivation of Intracellular Molecules by Fast-maturating Photosensitizing Fluorescence Protein, HyperNova. *Commun. Biol.* **2024**, *7*, 945.
(38) Takemoto, K.; Matsuda, T.; Sakai, N.; Fu, D.; Noda, M.; Uchiyama, S.; Kotera, I.; Arai, Y.; Horiuchi, M.; Fukui, K.; Ayabe, T.; Inagaki, F.; Suzuki, H.; Nagai, T. SuperNova, a Monomeric Photosensitizing Fluorescent Protein for Chromophore-assisted Light Inactivation. *Sci. Rep.* **2013**, *3*, 2629.
(39) Bulina, M. E.; Chudakov, D. M.; Britanova, O. V.; Yanushevich, Y. G.; Staroverov, D. B.; Chepurnykh, T. V.; Merzlyak, E. M.; Shkrob, M. A.; Lukyanov, S.; Lukyanov, K. A. A Genetically Encoded Photosensitizer. *Nat. Biothechnol.* **2006**, *24*, 95−99.
(40) Carpentier, P.; Violot, S.; Blanchoin, L.; Bourgeois, D. Structural Basis for the Phototoxicity of the Fluorescent Protein KillerRed. *FEBS Lett.* **2009**, *583*, 2839−2842.
(41) Pletnev, S.; Gurskaya, N. G.; Pletneva, N. V.; Lukyanov, K. A.; Chudakov, D. M.; Martynov, V. I.; Popov, V. O.; Kovalchuk, M. V.; Wlodawer, A.; Dauter, Z.; Pletnev, V. Structural Basis for Phototoxicity of the Genetically Encoded Photosensitizer KillerRed. *J. Biol. Chem.* **2009**, *284*, 32028−32039.

https://doi.org/10.1021/acsnano.4c16847
ACS Nano 2025, 19, 7188−7201

(42) de Rosny, E.; Carpentier, P. GFP-Like Phototransformation Mechanisms in the Cytotoxic Fluorescent Protein KillerRed Unraveled by Structural and Spectroscopic Investigations. *J. Am. Chem. Soc.* **2012**, *134*, 18015−18021.
(43) Gorbachev, D. A.; Staroverov, D. B.; Lukyano, K. A.; Sarkisyan, K. S. Genetically Encoded Red Photosensitizers with Enhanced Phototoxicity. *Int. J. Mol. Sci.* **2020**, *21* (22), 8800.
(44) Strack, R. L.; Strongin, D. E.; Mets, L.; Glick, B. S.; Keenan, R. J. Chromophore Formation in DsRed Occurs by a Branched Pathway. *J. Am. Chem. Soc.* **2010**, *132*, 8496−8505.
(45) Violot, S.; Carpentier, P.; Blanchoin, L.; Bourgeois, D. Reverse pH-Dependence of Chromophore Protonation Explains the Large Stokes Shift of the Red Fluorescent Protein mKeima. *J. Am. Chem. Soc.* **2009**, *131*, 10356−10357.
(46) Gayda, S.; Nienhaus, K.; Nienhaus, G. U. Mechanistic Insights into Reversible Photoactivation in Proteins of the GFP Family. *Biophys. J.* **2012**, *103*, 2521−2531.
(47) Duan, C.; Adam, V.; Byrdin, M.; Ridard, J.; Kieffer-Jaquinod, S.; Morlot, C.; Arcizet, D.; Demachy, I.; Bourgeois, D. Structural Evidence for a Two-Regime Photobleaching Mechanism in a Reversibly Switchable Fluorescent Protein. *J. Am. Chem. Soc.* **2013**, *135*, 15841−15850.
(48) Cormack, B. P.; Valdivia, R. H.; Falkow, S. FACS-optimized Mutants of the Green Fluorescent Protein (GFP). *Gene* **1996**, *173*, 33−38.
(49) Szymczak, A. L.; Vignali, D. A. Development of 2A Peptide-based Strategies in the Design of Multicistronic Vectors. *Expert Opin. Biol. Ther.* **2005**, *5*, 627−638.
(50) Shaner, N. C.; Campbell, R. E.; Steinbach, P. A.; Giepmans, B. N. G.; Palmer, A. E.; Tsien, R. Y. Improved Monomeric Red, Orange and Yellow Fluorescent Proteins Derived from Discosoma sp. Red Fluorescent Protein. *Nat. Biotechnol.* **2004**, *22*, 1567−1572.
(51) Riani, Y. D.; Matsuda, T.; Takemoto, K.; Nagai, T. Green Monomeric Photosensitizing Fluorescent Protein for Photo-inducible Protein Inactivation and Cell Ablation. *BMC Biol.* **2018**, *16*, 50.
(52) Oliinyk, O. S.; Shemetov, A. A.; Pletnev, S.; Shcherbakova, D. M.; Verkhusha, V. V. Smallest Near-infrared Fluorescent Protein Evolved from Cyanobacteriochrome as Versatile Tag for Spectral Multiplexing. *Nat. Commun.* **2019**, *10*, 279.
(53) Nieuwenhuizen, R. P. J.; Lidke, K.; Bates, M.; Puig, D. L.; Grünwald, D.; Stallinga, S.; Rieger, B. Measuring Image Resolution in Optical Nanoscopy. *Nat. Methods* **2013**, *10*, 557−562.
(54) Wickert, U.; Mücke, N.; Wedig, T.; Müller, S. A.; Aebi, U.; Herrmann, H. Characterization of the *in vitro* Co-assembly Process of the Intermediate Filament Proteins Vimentin and Desmin: Mixed Polymers at All Stages of Assembly. *Eur. J. Cell Biol.* **2005**, *84*, 379−391.
(55) Yang, X.; Pabon, L.; Murry, C. E. Engineering Adolescence: Maturation of Human Pluripotent Stem Cell-derived Cardiomyocytes. *Circ. Res.* **2014**, *114*, 511−523.
(56) Robison, P.; Caporizzo, M. A.; Ahmadzadeh, H.; Bogush, A. I.; Chen, C. Y.; Margulies, K. B.; Shenoy, V. B.; Prosser, B. L. Detyrosinated Microtubules Buckle and Bear Load in Contracting Cardiomyocytes. *Science* **2016**, *352*, aaf0659.
(57) Jeziorowska, D.; Fontaine, V.; Jouve, C.; Villard, E.; Dussaud, S.; Akbar, D.; Letang, V.; Cervello, P.; Itier, J.-M.; Pruniaux, M.-P.; Hulot, J.-S. Differential Sarcomere and Electrophysiological Maturation of Human iPSC-Derived Cardiac Myocytes in Monolayer vs. Aggregation-Based Differentiation Protocols. *Int. J. Mol. Sci.* **2017**, *18*, 1173.
(58) Skorska, A.; Johann, L.; Chabanovska, O.; Vasudevan, P.; Kussauer, S.; Hillemanns, M.; Wolfien, M.; Jonitz-Heincke, A.; Wolkenhauer, O.; Bader, R.; Lang, H.; David, R.; Lemcke, H. Monitoring the Maturation of the Sarcomere Network: a Super-resolution Microscopy-based Approach. *Cell. Mol. Life Sci.* **2022**, *79*, 149.
(59) Querard, J.; Markus, T.-Z.; Plamont, M.-A.; Gauron, C.; Wang, P.; Espagne, A.; Volovitch, M.; Vriz, S.; Croquette, V.; Gautier, A.; Le Saux, T.; Jullien, L. Photoswitching Kinetics and Phase Sensitive Detection Add Discriminative Dimensions for Selective Fluorescence Imaging. *Angew. Chem., Int. Ed.* **2015**, *54*, 2633−2637.
(60) Schindelin, J.; Arganda-Carreras, I.; Frise, E.; Kaynig, V.; Longair, M.; Pietzsch, T.; Preibisch, S.; Rueden, C.; Saalfeld, S.; Schmid, B.; Tinevez, J.-Y.; White, D. J.; Hartenstein, V.; Eliceiri, K.; Tomancak, P. A.; et al. Fiji: an open-source platform for biological-image analysis. *Nat. Methods* **2012**, *9*, 676−682.
(61) Lu, K.; Wazawa, T.; Matsuda, T.; Shcherbakova, D. M.; Verkhusha, V. V.; Nagai, T. Near-infrared PAINT Localization Microscopy via Chromophore Replenishment of Phytochrome-derived Fluorescent Tag. *Commun. Biol.* **2024**, *7*, 473.
(62) Lian, X.; Hsiao, C.; Wilson, G.; Zhu, K.; Hazeltine, L. B.; Azarin, S. M.; Raval, K. K.; Zhang, J.; Kamp, T. J.; Palecek, S. P. Robust Cardiomyocyte Differentiation from Human Pluripotent Stem Cells via Temporal Modulation of Canonical Wnt Signaling. *Proc. Natl. Acad. Sci. U.S.A.* **2012**, *109*, E1848−E1857.
(63) Hamad, S.; Derichsweiler, D.; Papadopoulos, S.; Nguemo, F.; Šarić, T.; Sachinidis, A.; Brockmeier, K.; Hescheler, J.; Boukens, B. J.; Pfannkuche, K. Generation of Human Induced Pluripotent Stem Cell-derived Cardiomyocytes in 2D Monolayer and Scalable 3D Suspension Bioreactor Cultures with Reduced Batch-to-batch Variations. *Theranostics* **2019**, *9*, 7222−7238.

https://doi.org/10.1021/acsnano.4c16847
ACS Nano 2025, 19, 7188−7201